Available online at www.sciencedirect.com

SciVerse ScienceDirect

Ceramics International 39 (2013) 4427–4435

CERAMICS INTERNATIONAL

www.elsevier.com/locate/ceramint

Electrochemical preparation of ZrO_2 nanopowder: Impact of the pulse current on the crystal structure, composition and morphology

Mustafa Aghazadeh*, Mojtaba Hosseinifard

Department of Chemistry, Faculty of Science, Islamic Azad University, Shahr-e-Ray branch, Tehran, Iran

Received 2 August 2012; received in revised form 10 November 2012; accepted 10 November 2012
Available online 27 November 2012

Abstract

Formation of the negatively charged colloidal zirconia species i.e. $[ZrO]^-$ at the cathode surface and low adhesion of the hydroxide deposit to its surface are common problems in the cathodic electrodeposition of zirconia. Deposition experiments with the direct current mode led to the total spallation of the deposit from the cathode surface and no deposit was obtained in practice. In order to minimize these problems, pulse current deposition was applied in the electrodeposition of ZrO_2. The results showed that the control of the base electrogeneration and deposit formation on the cathode surface is achievable using the pulse current mode. The XRD analysis and SEM observations revealed that the crystal structure, phase content and surface morphology of the prepared zirconia powders are significantly affected by the variation of t_{off} or t_{on}/t_{off} ratio. This work clearly showed that the pulse current electrodeposition can be introduced as an alternative route in the ZrO_2 cathodic electrodeposition and preparation of its nanostructured powder.

Keywords: A. Powders; A. Calcination; B. Electron microscopy; D. ZrO_2: electrochemical preparation

1. Introduction

Zirconium oxide (ZrO_2), also called zirconia, is an important versatile ceramic material due to its novel physical–chemical properties. Its high melting point, refractoriness, low thermal conductivity, high strength, toughness, corrosion and abrasion resistance make it suitable for a wide range of technological applications [1–6].

Among the various physical–chemical techniques used for the production of nanostructured zirconia [7–16], electrochemical route, i.e., cathodic electrodeposition, can be applied, an attractive and effective method due to its powerful control on the structural and morphological properties of the products. In this technique, metal hydroxide as a precursor is prepared by electrodeposition process and then converted into the metal oxide via heat-treatment. Up to now, various metal oxides such as ZrO_2 [17–23] and CeO_2 [24] thin films, Y_2O_3 nanoparticles, nanospheres and nanorods [25,26], La_2O_3 nanoplates [27], ZnO nanotubes [28] and NiO capsule-like particles [29] have been prepared using this technique.

The low adhesion of the zirconium hydroxide deposit to the cathode surface and film cracking has been reported as common difficulties during the cathodic electrodeposition of ZrO_2 from nitrate and/or chloride medium [20–23]. In cathodic electrodeposition, base (OH^-) electrogeneration imply an unusually large number of critical elementary phenomena or processes, which may occur simultaneously on the electrode surface. Hence, the adhesion of the deposit depends on the kinetics of the cathodic reductions including rate of gassing and the accompanied pH increase at the electrode surface [17,25]. The low adhesion of zirconium hydroxide films has been mainly attributed to the negative charge of the colloidal zirconium oxide (ZrO^-) particles formed in the high-pH region at the cathode surface as follows [23]:

In the first step, the cathodic reactions result in high-pH conditions at the cathode surface:

$$O_2 + 2H_2O + 4e^- \rightarrow 4OH^- \quad (1)$$

$$2H_2O + 2e^- \rightarrow H_2 + 2OH^- \quad (2)$$

*Corresponding author. Tel./Fax: +98 21 55229204.
E-mail address: Mustafa.aghazadeh@gmail.com (M. Aghazadeh).

0272-8842/$ - see front matter © 2012 Elsevier Ltd and Techna Group S.r.l. All rights reserved.
http://dx.doi.org/10.1016/j.ceramint.2012.11.036

In zirconyl chloride solution, the zirconyl salt ($ZrOCl_2 \cdot 8H_2O$) dissolves in water according to the following reaction [30]:

$$ZrOCl_2.8H_2O \rightarrow ZrO^{2+} + 2Cl^- + 8\,H_2O \quad (3)$$

The metal cations (ZrO^{2+}) are hydrated by water molecules to form a tetramer ($[Zr_4(OH)_8(H_2O)_{16}]^{8+}$), which is stable in the bulk solution. The tetramer consists of the four metal atoms in a square with double hydroxyl bridges linking them together. The tetramers show a tendency to release proton and form acidic bulk solutions:

$$[Zr_4(OH)_2\,(H_2O)_{16}]^{8+} \rightarrow [Zr(OH)_{2+x}.(4-x)H_2O]_4^{(8-4x)+} + 4xH^+ \quad (4)$$

In the next step, zirconium species are hydrolyzed by the electrogenerated base to form a colloidal oxide particle with a surface negative charge in the basic conditions at the cathode surface. The following surface reaction occurs at high pH region and so colloidal oxide particles with surface negative charge are formed:

$$Zr{-}OH + OH^- \rightarrow [Zr{-}O]^- + H_2O \quad (5)$$

The isoelectric point of hydrous zirconia has reported to be 6.7 [31]. Therefore, it could be assumed that the colloidal particles are negatively charged, which lead to a low adhesion of the deposit to the cathode surface and finally its spallation. This assumption can be also supported by the results of the electrodeposition experiments, which have been performed with pure $ZrOCl_2$ solutions by Zhitomirsky et al. [23]. In fact, they observed that the deposit spallation is occurred at deposition times exceeding 4 min, and no deposit is obtained at longer deposition durations. Furthermore, it has been reported that the Faradaic efficiency in the cathodic electrodeposition of ZrO_2 is low (approximately 20–40%) [17–20]. In these works, the observed low efficiencies have been attributed both to the reduction reactions that do not produce hydroxyl ions, and also to the formation of the hydroxide at the sites removed from the cathodic substrate due to the diffusion of the hydroxyl ions [17–19]. However, it seems that high rate of base electrogeneration and so excess of OH^- at the cathode surface are responsible for the observed low efficiencies at the applied deposition conditions. In previous works [32,33], we reported that the galvanostatic or direct current deposition of ZrO_2 at RT and also at elevated temperatures results no deposit on the cathode surface, whereas deposition experiments at low-bath temperature (10 °C) led to the formation of a thick deposit film on the cathode. These results clearly displayed that the bath temperature plays a key role in the cathodic electrodeposition of ZrO_2 via affecting the rate of the base electrogeneration, crystal growth process and kinetics of the zirconium hydroxide formation, such as diffusion and migration of zirconium cations as well as adhesion of the hydroxide deposit to the cathode and its spallation. It was also found that if the rate of base electrogeneration is more than the rate of deposit formation, the hydroxyl ions will be excess on the cathode surface and $[ZrO]^-$ species formed on the cathode so that the deposit spallatted from the surface. Hence, the low-temperature electrodeposition was introduced as a solution and effective route to overcome the mentioned problems in the cathodic electrodeposition of ZrO_2 [32,33]. Using this route, ultrafine nanoparticles, nanospheres and nanocapsules of ZrO_2 were successfully prepared and characterized.

In the present work, we introduced the pulse current (PC) electrodeposition as an effective route in the electrodeposition of ZrO_2 and preparation of its nanostructures. It should be noted that PC electrodeposition has been previously applied in the cathodic electrodeposition of ZrO_2 coatings or thin films on the stainless steel by Setare et al. [34]. In fact, they showed that the uniform and dense films of ZrO_2 are achievable by PC deposition. To our knowledge, PC cathodic deposition of metal oxides has been rarely studied, and only a few reports including pulse current deposition of WO_3–TiO_2 composite films [35,36] and Pb–Tl-oxides [37] are available in the literature. Pulse current electrodeposition has three independent variables, namely: (i) on-time (t_{on}), (ii) off-time (t_{off}) and (iii) peak current density (I_P), which are defined as below:

$$\theta = t_{on}/(t_{on}+t_{off}), f = 1/(t_{on}+t_{off}), I_a = I_p \times \left(t_{on}/(t_{on}+t_{off})\right) = I_p \times \theta \quad (6)$$

The main objective of the present work is the feasibility study of the preparation of ZrO_2 nanostructured powder via PC cathodic electrodeposition.

2. Experimental procedure

ZrO_2 cathodic electrodeposition experiments were carried out in a three-electrode system by applying the current density of 1 mA cm^{-2} in both direct and pulse current modes. The electrochemical cell includes a cathodic stainless steel substrate (316 L) centered between two parallel graphite anodes. An Ag/AgCl (KCl, saturated) electrode was used as the reference electrode. An additive-free aqueous solution of $ZrOCl_2 \cdot 8H_2O$ (0.01 M, Merck) was used as the electrolyte. Prior to each deposition, steel electrodes were galvanostatically electropolished at a current density of 0.5 A cm^{-2} for 5 min in a bath (70 °C) containing 50 vol% phosphoric acid, 25 vol% sulfuric acid and balanced deionized water. Additionally, in order to investigate the effects of the applied current modes (pulse or direct) on the kinetic of the base electrogeneration and the deposit formation, the cathode potential and pH were recorded during the electrodeposition experiments. All the experiments were carried out using an electrochemical workstation system (Potentiostat/Galvanostat Model: BHP-PGS 2066). The deposition experiments were conducted in the modes of direct and pulse current deposition with an equal applied charge (q=60 C). Direct current electrodeposition was carried out at the constant current density of 1 mA cm^{-2} for 10 min. The pulse current deposition experiments were also performed at two typical on-times and off-times listed in Table 1. Both DC and PC electrodeposition experiments were done at RT conditions. After electrodeposition, the steel was

Table 1
DC and PC deposition conditions of ZrO_2 from zirconyl chloride solution.

Sample name	Frequency, f (Hz)	Duty cycle, θ (%)	On-time, t_{on} (ms)	Off-time, t_{off} (ms)	t_{on}/t_{off}	Average current density, I_a (mA cm^{-2})	Deposition time ($_{min}$)	Current efficiency (%)
ZrOH-1 ZrO-1	100	50	5	5	1	0.5	20	64
ZrOH-2 ZrO-2	50	25	5	15	0.33	0.25	40	82
No deposit was obtained	dc current density: 1 mA cm^{-2}						10	0

washed several times with double-distilled water and dried at room temperature for 48 h. Then the electrolytic deposits were scraped from the electrodes and the obtained hydroxide powders were subjected to further analysis and also heat treatment at 700 °C in dry air atmosphere. The phase content and crystal structure of the samples were determined by X−ray diffraction (XRD) with a diffractometer (Phillips, PW-1800) using monochromatized Cu Kα radiation at a scanning speed of 5°/min. Thermogravimetric analysis (TGA) of the hydroxide samples was investigated by means of differential scanning calorimeter (DSC, STA-1500). Morphology of the samples was examined using a scanning electron microscope (SEM, Philips 515).

3. Results and discussion

3.1. Effects of the pulse current on the ZrO_2 electrodeposition

The electrochemical growth of $Zr(OH)_4$ deposit from an additive-free $ZrOCl_2 \cdot 8H_2O$ (0.01 M) aqueous electrolyte is achieved at the cathode through a mechanism of base (OH^-) electrogeneration, according to the cathodic reactions (1) and (2). By increasing the $OH^{\square}$ concentration to the required conditions in the reaction (7), $Zr(OH)_4$ will form and deposit on the cathode:

$$Zr^{4+}(aq) + 4OH^- \rightleftarrows Zr(OH)_4(s) \quad Ksp = [Zr^{4+}].[OH^-]^4 = 10^{-49} \tag{7}$$

Fig. 1 shows the variation of the potential during the $Zr(OH)_4$ deposition from chloride bath at both modes of direct and pulse current. The observed potential values (−1.15 V, −0.99 V and −0.96 V for DC and PC modes, respectively) suggest that the reduction of water (Eq. (2)) has a major role in the production of OH^- at our experimental conditions. In fact, the electrochemical step proceeds via reaction (2) at both modes. Fig. 2 shows variations of the pH at the cathode surface during the deposition of $Zr(OH)_4$ at both modes. These curves clearly indicate that pH at the cathode surface is quickly increased at the initial times of the deposition due to the base electrogeneration from the electrochemical step (reactions (1) and (2)) (as schematically shown in Fig. 3a). It should be noted that the rate of base generation in the DC mode is higher in comparison to the PC mode as one can obviously see from the slope of the pH curves in Fig. 2. In fact, the electrochemical reactions are off during the off-times in PC mode, and no base is generated. By increasing the pH at the cathode surface at longer deposition times, the conditions are ready for the chemical step and zirconium hydroxide starts to form and deposit on the cathode. These time can be referred to the deposition starting points. In fact, at these points, the OH^- produced from the electrochemical step starts to be consumed in the chemical step according to the following reactions (as shown schematically in Fig. 3b):

$$Zr^{4+}(aq) + 4OH^-(aq) + yH_2O \rightarrow [Zr(OH)_4.yH_2O] \downarrow \tag{8}$$

$$Zr^{4+}(aq) + xCl^-(aq) + (4-x)OH^-(aq) \rightarrow [Zr(OH)_{(4-x)}(Cl)_x.yH_2O] \downarrow \tag{9}$$

Deposit formation via reaction (9) can result in the chloride ion intercalation in the hydroxide deposit structure. Thus both zirconium hydroxide and zirconium hydroxide-chloride compositions are expected for the obtained deposits. From Fig. 2, it is seen that the chemical step is approximately started at the times of the 60 s, 110 s and 150 s after running the experiments (starting points of deposition, as shown in Fig. 2). Due to the low rate of base electrogeneration in the PC mode, these points are observed at longer times compared to the DC mode. After these points, the electrogenerated base in electrochemical step is subsequently consumed at the chemical step and the slope of the pH curves is lowered (as seen in Fig. 2). Thus it is expected that the amount of pH on the cathode surface is remained approximately constant. However, it should be noted that the level of pH on the cathode surface is mainly determined by the applied current density. From Fig. 2, it is seen that the slope of the pH curve in the DC mode is increased even after the starting point of deposition. This fact reveals that the rate of OH^- generation in the DC mode is faster than its consumption at all times during the deposition. Thus, it is possible that a fraction of OH^- can contribute to Eq. (5), resulting the deposit spallation (as shown in Fig. 3c). Also, it is possible that a fraction of OH^- ions is transported away from the surface, which results the low adhesion of the deposit. When a current pulse is exerted into the electrodeposition bath, a negatively charged layer is formed around the cathode as the process continues. When using DC, this layer charges to a

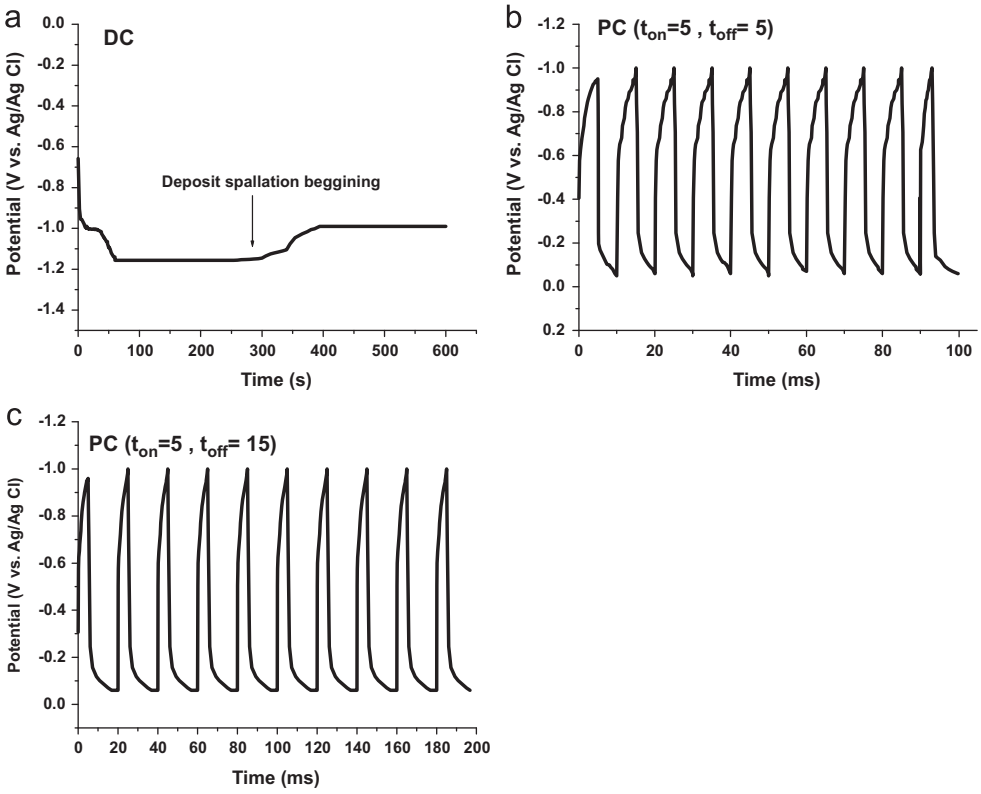

Fig. 1. Variations of the cathode potential during the DC (a) and PC (b and c) electrodeposition of ZrO_2.

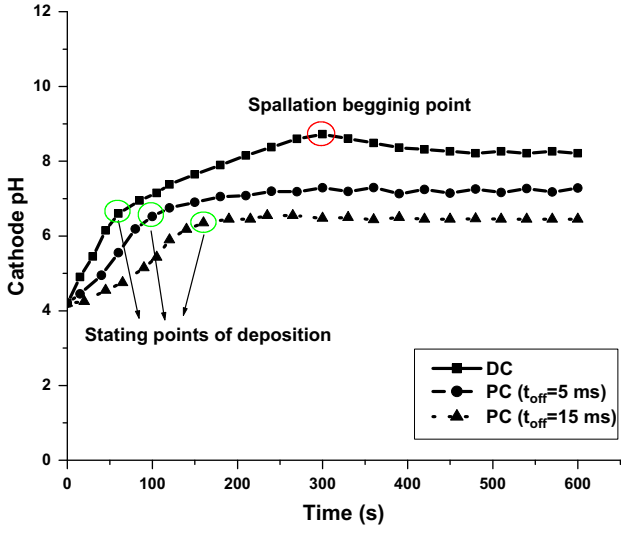

Fig. 2. Variations of the cathode pH during the DC (a) and PC (b and c) electrodeposition of ZrO_2.

defined thickness and obstructs the ions from reaching the cathode surface. In contrast to DC, PC experiments result in a thick deposit film on the cathode in practice. It seems that the pulse electrodeposition has been provided better conditions for the deposition. From Fig. 2, it is clearly seen that the pH variations or base content at the cathode surface is completely controlled during the PC deposition, which can be related to the sufficient time for the consumption of OH^- at the off-times. Thus formation of $[ZrO]^-$ species is less possible. Furthermore, in pulse electrodeposition, the output is periodically turned off, which allows the formation of OH^- layer on the cathode surface is discharged to some extent (as seen in Fig. 3d). This process is also allowed the Zr^{4+} ions to pass through the layer and onto the part more easily. During t_{off}, Zr^{4+} migrates to the depleted areas in the bath and more evenly distributed ions are available for deposition onto the cathode (Fig. 3d). Thus it can be concluded that the rate of the electrochemical step is more than the chemical step in the DC mode and therefore, deposit spallation is observed, and no deposit is obtained in this mode. While, in PC mode, the rate of the electrochemical step is lower than the chemical step and, therefore, the electrodeposition process is successful. Hence, it can be said that the rate of base electrogeneration is a key factor in the successful deposition of ZrO_2 and can be easily controlled by applying the pulse current.

3.2. Crystal structure of the samples

The XRD patterns of the oxide samples prepared by the PC mode are shown in Fig. 4. Zirconium oxide can exist in three different phases [38,39]. The stable monoclinic phase (m-ZrO_2) is formed at low temperatures, which is converted into a tetragonal phase (t-ZrO_2) at 1200 °C, and finally into a cubic phase at 2370 °C [40]. The main XRD peaks for the monoclinic phase (m-ZrO_2) occur at $2\theta = 28.15°$ and 34.16° [41–43]. The XRD pattern of the ZrO-1 sample (Fig. 4a) can be easily

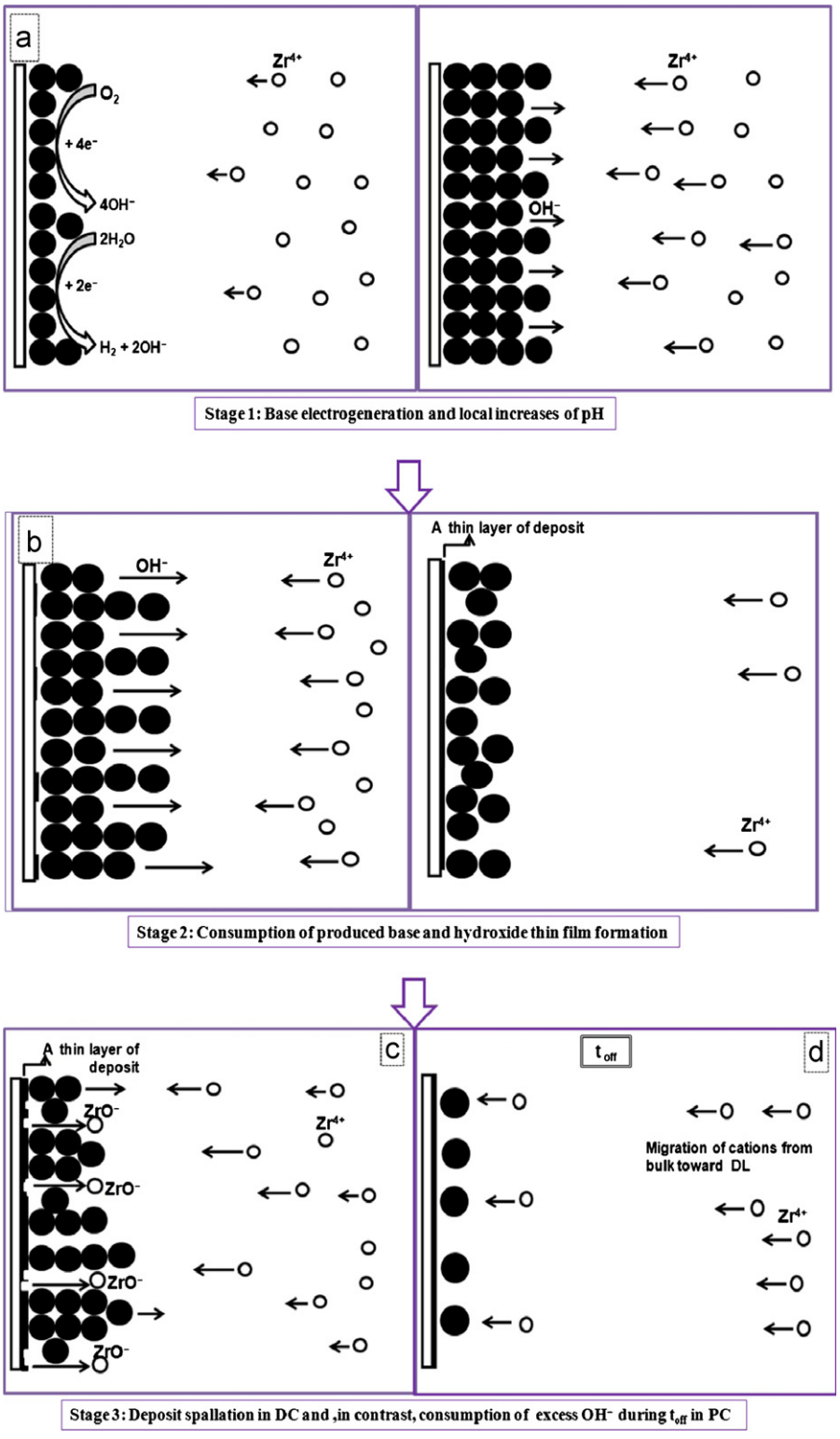

Fig. 3. Schematic of the stages of zirconium hydroxide deposition on the cathode surface from zirconyl chloride solution: (a) electrogeneration of base at the cathode surface by the reduction reaction of water and/or dissolved oxygen molecules, (b) local increasing the pH at the cathode surface and the hydroxide formation for deposition of thin hydroxide layer on the cathode surface, (c) spallation of deposit from the cathode surface due to the formation of ZrO^- species in the DC mode and (d) consumption of excess OH^- during the off-time in the PC mode.

assigned to *m*-ZrO_2 with lattice constants, $a=0.5313$ nm, $b=0.5213$, $c=0.5147$ nm and $\beta=99.228$ and are in good agreement with those of the standard data (JCPDS card No. 37-1484) and without having any extra diffraction lines from any impurities or other phases. Almost all the diffraction peaks with similar relative intensity as suggested

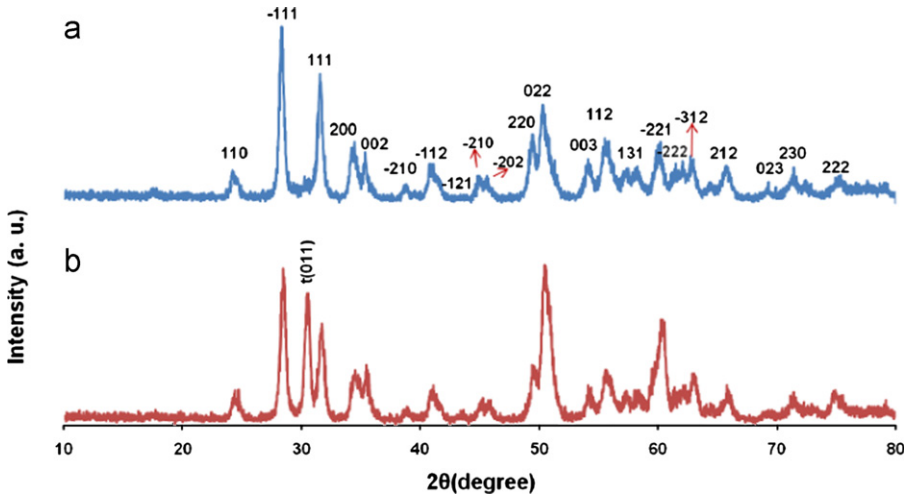

Fig. 4. XRD patterns of the prepared oxide samples; (a) ZrO-1 and (b) ZrO-2.

Table 2
The results of hermogravimetric analysis of the hydroxide samples prepared by PC mode.

Sample name	Off-time, t_{off} (ms)	Physically absorbed water (%)	Structural water (%)	Total weight loss (%)	Estimated chemical formula
ZrOH-1	5	15.01	10.16	25.12	$Zr(OH)_4$ 1.19 H_2O
ZrOH-2	15	15.16	12.34	27.49	$Zr(OH)_4$ 1.20 H_2O

in the standard data are observed in the experimental XRD pattern and are significantly sharp, hence confirming the purity and high crystallinity of the prepared ZrO-1 sample. Moreover, all the prominent peaks with sufficient peak intensity are indexed as shown in Fig. 4a. The XRD pattern of ZrO-2 sample (Fig. 4b) shows one diffraction peak at $2\theta = 31.5^{\circ}$. This peak, i.e., (011), can be related to the tetragonal phase (t-ZrO_2) [42,44], while the others easily correspond to m-ZrO_2. The relative amounts of m- and t-ZrO_2 phases in the ZrO-2 sample can be calculated using the following expression [12,45]:

$$\%m\text{-}ZrO_2 = \frac{(I_{m(11\bar{1})}) + (I_{m(111)}) \times 100}{(I_{m(11\bar{1})}) + (I_{m(111)}) + I_{t(011)}} \quad (10)$$

where I is the intensity of the diffraction peak. The amount of t-ZrO_2 was calculated to be approximately 37%. This finding shows that the phase content of the oxide samples is affected by the pulse parameters, i.e., t_{on}/t_{off} ratios so that the metastable t-ZrO_2 can be prepared in lower t_{on}/t_{off} ratio. It should be noted that the structural properties of the oxide products may be affected by heat treatment. However, the structural and morphological properties of both products are essentially originated from their hydroxide precursors which have been heated under the same thermal conditions. As a result, it can be said that the pulse parameters directly dictate the properties of the oxide products. It seems that the deposit has been better nucleated and crystallized in longer off-times. According to Ref. [12,46,47], it can be expected that the t-ZrO_2 could be formed when the size of crystallites is lower than the critical value of about 10 nm. Transformation to the m-ZrO_2 could be observed when the size of the tetragonal crystallites exceeds this critical value. The average crystallite size (D) of the samples was calculated from the width of the (-111) peak through using the Scherrer equation ($D = 0.9\lambda/\beta \cos\theta$), where, λ is the wavelength of X-ray radiation, θ is the Bragg angle of the peak and β (FWHM) is defined as the full-width at half maximum of the diffraction peak in radians. The crystallite sizes of the ZrO-1 and ZrO-2 samples were calculated to be around 15 and 8 nm, respectively

3.3. DCS-TGA

The thermal behavior of the hydroxide samples during the heat treatment process was investigated by DCS-TGA analysis and the results are listed in Table 2. As can be seen in DSC curves (Fig. 5a), both samples (ZrOH-1 and ZrOH-2) show two distinct peaks during the heat treatment process, i.e., an endothermic one at temperatures of below 200 °C followed by a broad exothermic peak with a sharp maximum at 470 °C. The endothermic peak is related to the required heat for the evaporation or loss of physically absorbed water from [Zr (OH) $_4 \cdot xH_2O$] precursor, dehydroxylation of hydroxyl groups from $Zr(OH)_4$ and/or the gradual decomposition of the structural water. Accordingly, TG curves of both samples (Fig. 5b) show a considerable weight loss between 50 and 200 °C, which is due to these dehydrations. The exothermic peak in the DSC curves of both samples is attributed to the phase transformation of tetragonal to the monoclinic form of ZrO_2 [8,17,35] without substantial weight loss. The total weight loss and estimated formula for the

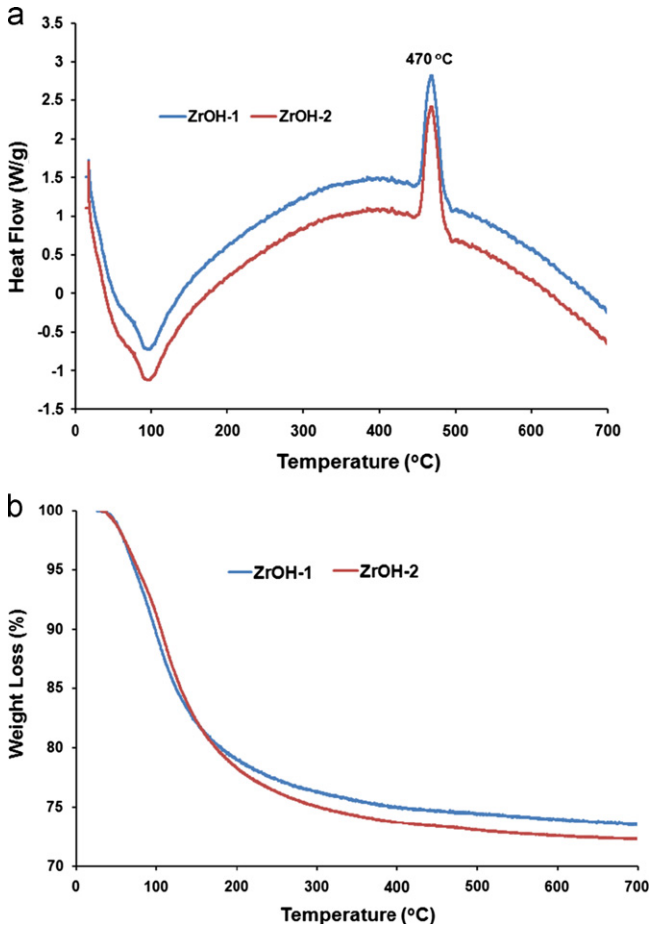

Fig. 5. DSC (a) and TG (b) curves of the deposited hydroxide samples; (a) ZrOH-1 and (b) ZrOH-2.

samples are listed in Table 2. The sample prepared at longer off-time (ZrOH-2 sample) has more total weight loss and absorbed water compared with the ZrOH-1 sample. This may be originated from the low kinetic of the deposit formation, which allowed the chloride ions to intercalate in the deposit structure. Finally, the following sequence can be proposed to interpret the observed structural changes during the heat treatment of both samples:

$$Zr(OH)_4.xH_2O \overset{150^{\circ}C}{\rightarrow} Zr(OH)_4 \overset{350^{\circ}C}{\rightarrow} t-ZrO_2 \overset{470^{\circ}C}{\rightarrow} m-ZrO_2 \quad (11)$$

3.4. Morphology

Figs. 6 and 7 show the surface morphology of the prepared hydroxide and oxide samples, respectively. As seen in SEM images, the surface morphologies and continuity of both hydroxide deposits were significantly affected by the variation of t_{off} or t_{on}/t_{off} ratio. The SEM images of ZrOH-1 sample (Fig. 6a, b) as well as ZrO-1 (Fig. 6c, d) display the uneven surface and completely agglomerated particles with an average particle size of 40 nm. In fact, the micrographs of ZrOH-1 sample (Fig. 6a, b) exhibit an irregular morphology with large cavities, which can be attributed to the H_2 bubbling observed in the electrochemical step. The surface morphology of the ZrOH-2 sample (Fig. 7a, b) is rather homogeneous, which suggests that the deposit formation has occurred under uniform levels of current distribution. This sample is largely composed of spherical agglomerates with grain sizes of about 400 nm. Higher magnification of hydroxide sample (Fig. 7b) reveals that the large agglomerates are composed of tiny semi-spherical agglomerates with

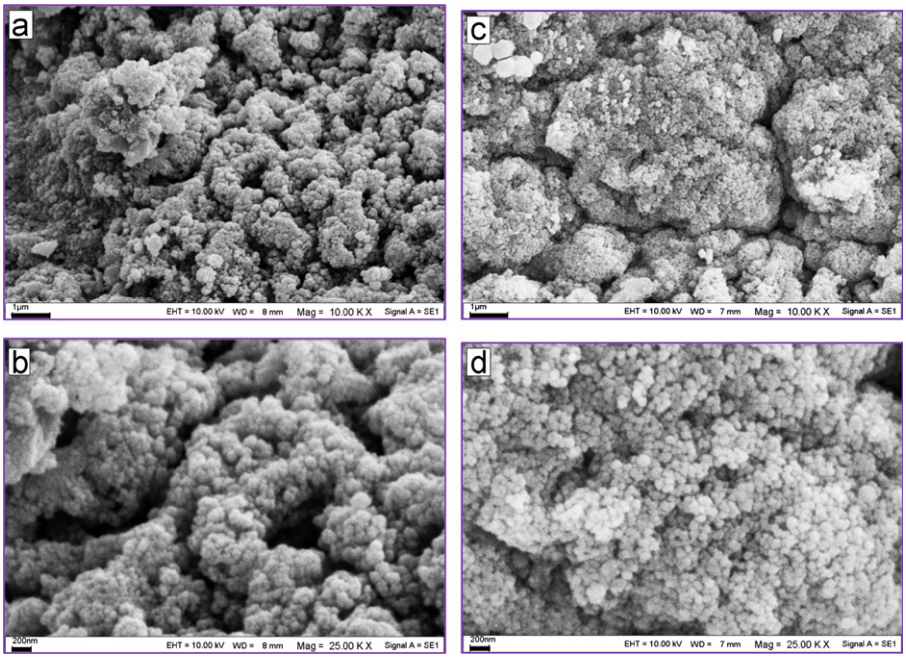

Fig. 6. SEM images of the prepared ZrOH-1(a and b) and ZrO-1 (c and d) samples.

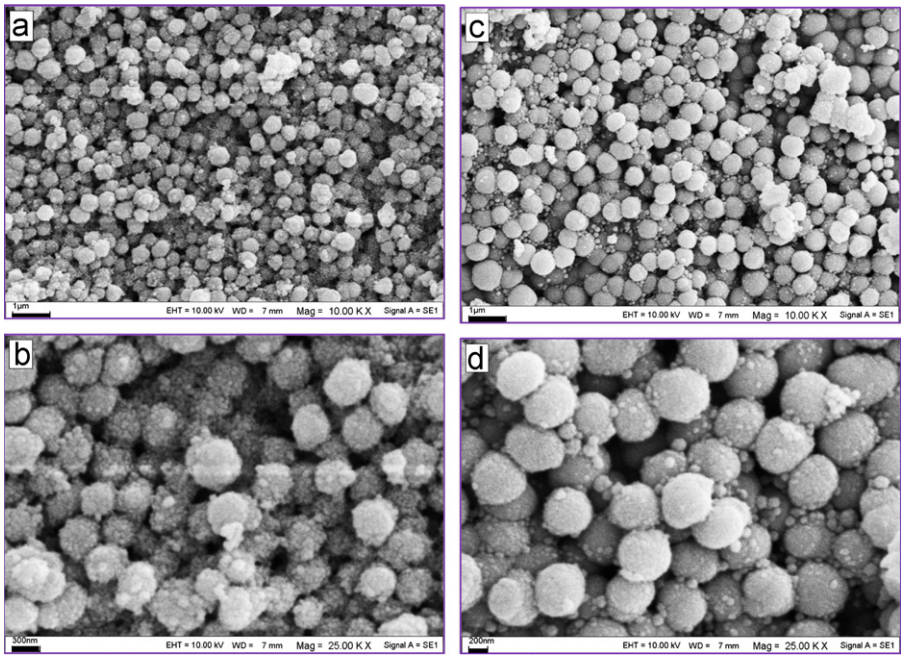

Fig. 7. SEM images of the prepared ZrOH-2 (a and b) and ZrO-2 (c and d) samples.

an average size of nearly 20 nm. Due to the surface forces, these particles stick together to form larger agglomerates, which are the thermodynamically more stable phase of ZrO_2 (*m*-ZrO_2). In addition, ZrOH-2 sample exhibits more coherent structure with denser packing and reduced number of cavities. This may be attributed not only to a more uniform distribution of the applied current but also to a reduced mass transfer limitation during the deposit formation as a result of longer off-time (lower duty cycle or lower t_{on}/t_{off} ratio). After annealing of this sample at 700 °C, nearly mono-dispersed oxide particles were obtained (Fig. 7c, d). From Fig. 7d, it is seen that the annealed sample composed of well-dispersed spherical particles with average diameters of 400 nm. These results clearly show the effects of pulse parameters on the microstructure of the prepared ZrO_2 samples.

Based on the findings in this work, it can be concluded that the pulse current deposition opens a new and effective route for the cathodic electrodeposition of ZrO_2 and preparation of its nanostructures. Through this method, one can easily overcome the mentioned problems in the synthesis of ZrO_2. It should be noted that, a systematic study of correlation between the pulse parameters (pulse frequency and duty cycle) and the structural and morphological properties of ZrO_2 is currently being done.

4. Conclusion

In summary, the pulsed current electrodeposition was proposed as an alternative route in the cathodic electrodeposition of nanostructured ZrO_2 powder without encountering any problems, i.e., formation of the negatively charged species, low adhesion of the deposit and its spallation. By using this method, nanoparticles and nanospheres of ZrO_2 were successfully prepared and characterized.

References

[1] M.J. Bannister, W.G. Garrett, Production of stabilized zirconia for use as a solid-state electrolyte, Ceramics International 1 (1975) 127–133.
[2] D. Stöver, H.P. Buchkremer, S. Uhlenbruck, Processing and properties of the ceramic conductive multilayer device solid oxide fuel cell (SOFC), Ceramics International 30 (2004) 1107–1113.
[3] G.A. Gogotsi, E.E. Lamonova, Y.A. Furmanov, I.M. Savitskaya, Zirconia crystals suitable for medicine: 1. Implants, Ceramics International 20 (1994) 343–348.
[4] T. Yamaguchi, Application of ZrO_2 as a catalyst and a catalyst support, Catalysis Today 20 (1994) 199–217.
[5] W.H. Tuan, J.R. Chen, C.J. Ho, Critical zirconia amount to enhance the strength of alumina, Ceramics International 34 (2008) 2129–2135.
[6] J.A. Sawicki, Evidence of Ni_2FeBO_5 and *m*-ZrO_2 precipitates in fuel rod deposits in AOA-affected high boiling duty PWR core, Journal of Nuclear Materials 347 (2008) 248–269.
[7] C.Y. Chen, T.K. Tseng, S.C. Tsai, C.K. Lin, H.M. Lind, Effect of precursor characteristics on zirconia and ceria particle morphology in spray pyrolysis, Ceramics International 34 (2008) 409–416.
[8] M. Chatterjee, J. Ray, A. Chatterjee, D. Ganguli, High purity zirconia powders via wet chemical processing: a comparative study, Ceramics International 18 (1992) 337–342.
[9] J. Chandradass, M. Balasubramanian, Sol–gel processing of alumina–zirconia minispheres, Ceramics International 31 (2005) 743–748.
[10] T. Ogihara, N. Mizutani, M. Kato, Processing of monodispersed ZrO_2 powders, Ceramics International 13 (1987) 35–40.
[11] Y. Huang, T. Ma, J.L. Yang, L.M. Zhang, J.T. He, H.F. Li, Preparation of spherical ultrafine zirconia powder in microemulsion system and its dispersibility, Ceramics International 30 (2004) 675–681.

[12] Y. Suyama, T. Mizobe, A. Kato, ZrO_2 powders produced by vapor phase reaction, Ceramics International 3 (1977) 141–146.
[13] I. Haase, L. Yib, E.M. Nicht, H. Xiaoxian, G. Jinkun, Preparation and characterization of ultrafine zirconia powder, Ceramics International 18 (1992) 343–351.
[14] L. Kumari, G.H. Du, W.Z. Li, R.S. Vennila, S.K. Saxena, D.Z. Wang, Synthesis, microstructure and optical characterization of zirconium oxide nanostructures, Ceramics International 35 (2009) 2401–2408.
[15] S. Kongwudthitia, P. Praserthdam, P. Silveston, M. Inoue, Influence of synthesis conditions on the preparation of zirconia powder by the glycothermal method, Ceramics International 29 (2003) 807–881.
[16] N. Garg, V.K. Mittal, S. Bera, A. Dasgupta, V. Sankaralingam, Preparation and characterization of tetragonal dominant nanocrystalline ZrO_2 obtained via direct precipitation, Ceramics International 38 (2012) 2507–2512.
[17] R. Chaim, I. Silberman, L. Gal-Or, Electrolytic ZrO_2 coatings I. electrochemical aspects, Journal of the Electrochemical Society 138 (1991) 1939–1942.
[18] S.K. Yen, Characterization of electrolytic ZrO_2 coating on AISI 316L stainless steel, Journal of the Electrochemical Society 146 (1999) 1392–1396.
[19] S.K. Yen, Mechanism of electrolytic ZrO_2 coating on commercial pure titanium, Materials Chemistry and Physics 63 (2000) 256–262.
[20] I. Zhitomirsky, A. Petric, Electrolytic deposition of zirconia and zirconia organoceramic composites, Materials Letters 46 (2000) 1–6.
[21] I. Zhitomirsky, A. Petric, Electrolytic deposition of ZrO_2–Y_2O_3 films, Materials Letters 50 (2001) 189–193.
[22] I. Avramova, D. Stoychev, T. Marinova, Characterization of a thin CeO_2–ZrO_2–Y_2O_3 films electrochemical deposited on stainless steel, Applied Surface Science 253 (2006) 1365–1370.
[23] X. Pang, I. Zhitomirsky, M. Niewczas, Cathodic electrolytic deposition of zirconia films, Surface and Coatings Technology. 195 (2005) 138–146.
[24] I. Zhitomirsky, A. Petric, Electrochemical deposition of ceria and doped ceria films, Ceramics International 27 (2001) 145–155.
[25] M. Aghazadeh, A.A. Malek Barmi, H.M. Shiri, Cathodic electrodeposition of $Y(OH)_3$ and Y_2O_3 nanostructures from chloride bath. Part II: effect of the bath temperature on the crystal structure, composition and morphology, Ceramics International (2012) Accepted.
[26] M. Aghazadeh, A. Nozad, H. Adelkhani, M. Ghaemi, Synthesis of Y_2O_3 nanospheres *via* heat-treatment of cathodically grown $Y(OH)_3$ in chloride medium, Journal of the Electrochemical Society 157 (2010) D519–522.
[27] M. Aghazadeh, A. Nozad, M. Ghaemi, T. Yousefi, La_2O_3 nanoplates prepared by heat-treatment of electrochemically grown $La(OH)_3$ nanocapsules from nitrate medium, Journal of the Electrochemical Society 158 (2011) E136–E141.
[28] J. Yang, Y. Lin, Y. Meng, Y. Liu, A two-step route to synthesize highly oriented ZnO nanotube arrays, Ceramics International 38 (2012) 4555–4559.
[29] H.M. Shiri, M. Aghazadeh, Synthesis, characterization and electrochemical properties of capsule-like NiO nanoparticles, Journal of the Electrochemical Society 159 (2012) E132–E138.
[30] A. Clearfield, The mechanism of hydrolytic polymerization of zirconyl solutions, Journal of Materials Research 5 (1990) 161–162.
[31] G.A. Parks, The isoelectric points of solid oxides, solid hydroxides, and aqueous hydroxo complex systems, Chemical Reviews 65 (1965) 177–198.
[32] M. Aghazadeh, Cathodic electrodeposition of ZrO_2: Impact of current density on the crystal structure, composition and morphology, Journal of the Electrochemical Society 159 (2012) E53–E58.
[33] M. Aghazadeh, A.A. Malek Barmi, M. Hosseinifard, Nanoparticulates $Zr(OH)_4$ and ZrO_2 prepared by low-temperature cathodic electrodeposition, Materials Letters 73 (2012) 28–31.
[34] E. Setare, K. Raeissi, M.A. Golozar, M.H. Fathi, The structure and corrosion barrier performance of nanocrystalline zirconia electrodeposited coating, Corrosion Science 51 (2009) 1802–1808.
[35] N.R. de Tacconi, C.R. Chenthamarakshan, K. Rajeshwar, T. Pauport, D. Lincot, Pulsed electrodeposition of WO_3–TiO_2 composite films, Electrochemistry Communications 5 (2003) 220–224.
[36] S. Somasundaram, C.R. Chenthamarakshan, N.R. de Tacconi, N.A. Basit, K. Rajeshwar, Composite WO_3–TiO_2 films: pulsed electrodeposition from a mixed bath versus sequential deposition from twin baths, Electrochemistry Communications 8 (2006) 539–543.
[37] J.A. Switzer, M.J. Shane, R.J. Phillips, Electrodeposited ceramic superlattices, Science 247 (1990) 444–446.
[38] C. Piconi, G. Maccauro, Zirconia as a ceramic biomaterial, Biomaterials 20 (1999) 1–25.
[39] A.M. Alper, in: J.L. Margrave (Ed.), High Temperatures Oxides, Part II: Oxides of Rare Earths, Titanium, Zirconium, Hafnium, Niobium and Tantalum, vol. 5-II, Academic Press, New York, 1970.
[40] A.E. Bohe, J. Andrade-Gamboa, D.M. Pasquevich, A.J. Tolley, J.L. Pelegrina, Microstructural characterization of ZrO_2 particles prepared by reaction of gaseous $ZrCl_4$ with Fe_2O_3, Journal of the American Ceramic Society 83 (2000) 755–760.
[41] E.O. Bensadon, P.A.P. Nascente, P. Olivi, L.O.S. Bulhoes, E.C. Pereira, Cubic stabilized zirconium oxide anodic films prepared at room temperature, Chemistry of Materials 11 (1999) 277–280.
[42] C.K. Lin, C.M. Zhang, J. Lin, Phase transformation and photoluminescence properties of nanocrystalline ZrO_2 powders prepared *via* the pechini-type sol – gel process, Journal of Physical Chemistry 111C (2007) 3300–3307.
[43] H. Habazaki, K. Shimizu, S. Nagata, K. Asami, K. Takayama, Y. Oda, P. Skeldon, G.E. Thompson, Inter-relationship between structure and dielectric properties of crystalline anodic zirconia, Thin Solid Films 479 (2005) 144–151.
[44] P. Salas, E. De La Rosa-Cruz, L.A. Diaz-Torres, V.M. Castano, R. Melendrez, M. Barboza-Flores, Monoclinic ZrO_2 as a broad spectral response thermoluminescence UV dosemeter, Radiation Measurements 37 (2003) 187–190.
[45] B.B.S. Reddy, K. Das, A.K. Datta, S. Das, Pulsed co-electrodeposition and characterization of Ni based nanocomposites reinforced with combustion-synthesized, undoped, tetragonal-ZrO_2 particulates, Nanotechnology 19 (2008) 115603, http://dx.doi.org/10.1088/0957-4484/19/11/115603.
[46] R.C. Garvie, M.F. Goss, Intrinsic size dependence of the phase transformation temperature in zirconia microcrystals, Journal of Materials Science 21 (1986) 1253–1257.
[47] R.C. Garvie, P.S. Nicholson, Phase analysis in zirconia systems, Journal of the American Ceramic Society 55 (1972) 303–305.